STUDY ON ORTHOGONAL STRAIN CHARACTERISTICS OF BRASSICA NAPUS STEMS DURING TENSILE PROCESS BASED ON DIGITAL IMAGE CORRELATION

/

基于 DIC 的油菜茎秆拉伸过程正交应变特性试验研究

Guangchao ZHAN[1], Yi YANG[1], Guodang LIAN*[2], Peng ZHANG[1], Wangyuan ZONG[3]

[1] School of Electromechanical and Intelligent Manufacturing, Huanggang Normal University, Huanggang 438000, Hubei, China

[2] School of Mechanical and Electrical Engineering, Lanzhou University of Technology, Lanzhou 730050, Gansu; China

[3]College of Engineering, Huazhong Agricultural University, Wuhan 430070, Hubei, China

Tel: +86-180-8650-1301; E-mail: guangchaozhan@hgnu.edu.cn

DOI: https://doi.org/10.35633/inmateh-79-79

***Keywords:** Brassica napus; stem biomechanics; orthogonal strain; digital image correlation*

ABSTRACT

The key challenge in Brassica napus combine harvesting is achieving a balance between threshing rate and impurity rate, both of which are strongly influenced by stem breakage. This study investigated the breakage characteristics and static mechanical properties of Brassica napus stems from the middle and lower reaches of the Yangtze River using axial tensile tests combined with digital image correlation (DIC). The results showed that the fiber layer area of rapeseed *stems increased with stem diameter, and stem breaking force was significantly positively correlated with stem diameter. For stem diameters ranging from 7 to 16 mm, the breaking force ranged from 166.82 to 970.82 N and was described by the relationship F_b=42.064d_{x1}-92.894. The tensile strength of rapeseed stems ranged from 25.1 to 64.6 MPa, and a quadratic response surface model relating tensile strength to stem diameter and moisture content was established. DIC measurements of strain in the radial and axial orthogonal directions showed that axial deformation was substantially smaller than radial deformation, with an average axial strain of $\varepsilon_y=4.22\pm2.23\times10^{-3}$ and an average radial strain of $\varepsilon_x=3.84\pm2.17\times10^{-2}$. These findings improve the understanding of the mechanical response of rapeseed stems under tensile loading and provide a theoretical basis for optimizing threshing devices for efficient, low-damage rapeseed harvesting.*

摘要

油菜联合收割中的核心挑战是平衡物料的脱净率与破碎率，而这直接受到茎秆破碎程度的影响。本研究针对长江中下游地区的油菜植株，通过轴向拉伸试验配合数字图像相关技术，深入探讨茎秆的破碎条件和静态特性。研究结果显示，油菜茎秆的纤维层的面积随着茎秆直径的增大而增大，茎秆的拉断力和茎秆直径呈显著正相关。在直径为 7 至 16 mm 的油菜茎秆中，拉断力介于 166.82 N 到 970.82 N 之间，其与直径的关系表达为：F_b=42.064d_{x1}-92.894。油菜茎秆的抗拉强度范围为 25.1 MPa 至 64.6 MPa，并建立了油菜茎秆的抗拉强度与油菜茎秆直径及含水率的二次响应面模型。使用数字图像技术对径向和轴向两个正交方向的应变进行测量，结果表明轴向变形显著小于径向变形，平均轴向应变为 $\varepsilon_y=4.22\pm2.23\times10^{-3}$，径向应变为 $\varepsilon_x=3.84\pm2.17\times10^{-2}$。这些结果不仅揭示了茎秆在受力过程中的机械响应规律，还为优化脱粒装置以实现高效低损伤的油菜籽收割提供了重要的理论依据。

INTRODUCTION

Brassica napus is a predominant oil crop in China, playing a pivotal role in ensuring the supply of edible vegetable oil and enhancing farmers' economic returns (*Sun et al., 2026; Guo et al., 2024; Mazzilli et al., 2024*). With the transformation of rapeseed production from merely establishing crop acreage to achieving high-quality harvesting, combine harvesting technology has emerged as a critical factor in enhancing production efficiency and reducing labor costs (*Li et al., 2025; Shu et al., 2025*). In a rapeseed combine harvester, the threshing device is the core component that directly processes the crop mixture consisting of seeds, pods, and stems. Its operating performance directly affects harvest loss, breakage rate, and the load on the cleaning system (*Zhang et al., 2025*).

Guangchao Zhan, Lecture, Ph.D.; Yi Yang, Lecture, Ph.D.; Guodang Lian, Associate Professor, Ph.D.; Peng Zhang, Lecture, Ph.D.; Wangyuan Zong, Professor, Ph.D.

Extensive research indicates that grain loss and cleaning burden during mechanized rapeseed harvesting are intrinsically linked to the mechanical properties and fracture behavior of plant organs such as stems and pods (*Qing et al., 2021*). However, the majority of existing studies have prioritized the optimization of threshing parameters and the evaluation of overall machine performance, while the biomechanical responses of the rapeseed stem itself under typical loading conditions have received comparatively less attention.

During the threshing process of rapeseed combine harvesting, the drum and concave apply repeated beating, rubbing, and compression actions on the material. Consequently, the stems are subjected not only to axial tension, bending, and shear loads but also to complex stress states coupled with transverse compression (*Vlădut et al., 2023; Zhan et al., 2025*). Insufficient stem breakage often leads to the entrapment of pods and grains, thereby reducing threshing and separation efficiency. Conversely, excessive stem fragmentation generates substantial quantities of short segments and fine fibers, significantly increasing the separation burden on the cleaning system, degrading the airflow field and screening conditions, and ultimately resulting in increased cleaning losses and energy consumption (*Zhou et al., 2025; Yuan et al., 2024*). Therefore, a systematic investigation into the deformation and failure laws of rapeseed stems under typical loads, such as tension, from a plant biomechanics perspective is essential. Acquiring a comprehensive understanding of their critical fracture conditions and anisotropic mechanical properties holds significant theoretical value and engineering utility for the structural design and parameter matching of threshing devices (*Tang et al., 2024; Cujbescu et al., 2021; Vlăduț et al., 2022*).

Currently, research regarding the mechanical properties of rapeseed plants primarily concentrates on overall flexural strength, bending modulus, and parameter calibration based on Discrete Element Method simulations (*Guo et al., 2024; Guan et al., 2022; Hu et al., 2025*). In the context of mechanized harvesting conditions, scholars have analyzed stem breaking forces, pod threshing forces, and grain damage mechanisms by combining experimental and simulation approaches (*Sun et al., 2025; Han et al., 2024; Shan et al., 2024*). Some studies have explored the viscoelastic properties and constitutive relationships of rapeseed stems, demonstrating that their mechanical performance is significantly influenced by factors such as variety, moisture content, and nodal structure (*Ren et al., 2014; Lian et al., 2022; Sikorska et al., 2023*). However, these studies predominantly rely on traditional loading and measurement techniques or simulation model assumptions. Consequently, the strain data obtained are typically limited to single-point or local measurements, rendering it challenging to elucidate the full-field deformation characteristics and strain distribution patterns of rapeseed stems, which are heterogeneous and anisotropic biomaterials, under complex loading conditions.

Digital Image Correlation is a non-contact full-field displacement and strain measurement method based on grayscale image matching, distinguished by high measurement precision, broad material applicability, and flexible experimental configuration. In recent years, DIC technology has been widely applied in mechanical testing of materials such as steel and composites, capable of acquiring full-field strain information on specimen surfaces under tensile, compressive, and fatigue loads (*Fang et al., 2026; Wang et al., 2023*). By analyzing speckle images on a material's surface, this method can effectively capture local strain concentrations and damage evolution during deformation, offering a novel technical approach for investigating the deformation and damage of heterogeneous materials like plant stems.

It is noteworthy that reports on the orthogonal strain characteristics of rapeseed stems during uniaxial tensile processes such as axial-radial strain response, cross-sectional anisotropy, and the coupling effects of hollow structures remain scarce. On one hand, rapeseed stems possess hollow, multi-layered tissue structures with distinct fiber orientations, exhibiting significant orthotropic anisotropic deformation characteristics under tensile loads (*Xiao et al., 2026; Han et al., 2024; Parvin et al., 2021*). On the other hand, traditional measurement methods face limitations in simultaneously acquiring full-field strain data in both axial and radial directions during the stretching process, thereby restricting quantitative in-depth analysis of orthogonal strain characteristics and failure mechanisms. Full-field strain measurement based on DIC allows for the synchronous observation and quantitative characterization of axial and radial strains in rapeseed stems during stretching without altering the force boundary conditions of the specimen, providing an effective means to reveal these orthogonal strain properties.

In summary, in light of the significant impact of stem crushing behavior on threshing and cleaning performance during rapeseed combine harvesting, and addressing the current lack of research on orthogonal strain characteristics under tensile conditions, this study aims to employ DIC technology to conduct full-field measurement and analysis of the axial and radial strains of rapeseed stems during the tensile process.

This research seeks to explore the laws governing orthotropic anisotropic deformation and their relationship with structural parameters, thereby providing a theoretical basis and experimental support for understanding the working mechanisms of rapeseed threshing devices and optimizing their design parameters.

MATERIALS AND METHODS

Test Materials and Equipment

Observation of the internal structure of *Brassica napus* plants showed that the rapeseed stem is mainly composed of an outer fiber layer and an inner pith. The rapeseed stem is approximately cylindrical with neatly arranged fiber layers, as shown in figure 1. Assuming that the mechanical parameters in all radial directions (representing the bonding force between fiber layers) are equal, and the axial mechanical parameters primarily consist of the tensile strength of the fibers, the rapeseed stem can be regarded as an orthotropic material similar to wood and bamboo. Therefore, this paper investigates the axial and radial mechanical properties of rapeseed stem respectively.

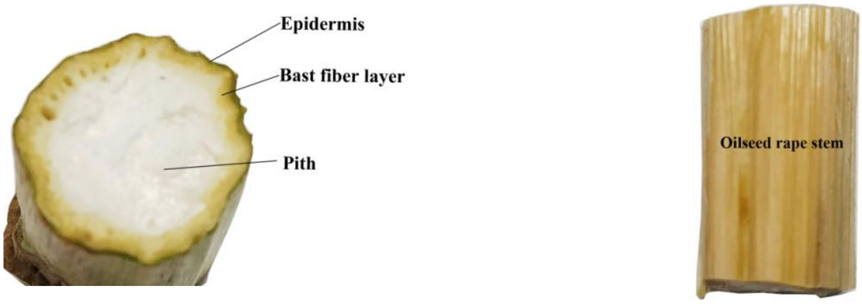

Fig.1 - Structure of rape stem

The test materials were mechanically precision-sown *Brassica napus* plants from the experimental field of Huazhong Agricultural University. The variety was *Brassica napus L*. 'Huayouza 62'. Three plots were randomly selected, and 12 rape plants were chosen from each plot. Healthy plants showing vigorous growth and free from pests or diseases were manually harvested. After harvesting, the rape stems were sectioned to obtain 200 mm segments below the first branch, with diameters ranging from 7 to 16 mm, to serve as the materials for tensile testing. To prevent moisture loss, the collected samples are stored in sealed bags.

Tensile tests were conducted on the rapeseed stems to determine their axial breaking force, tensile strength, and axial and radial deformation. The main equipment used during the testing process included: a universal material testing machine, a Kinect v2 camera, a laptop computer, a vernier caliper, a marker pen, label paper, an OHAUS moisture analyzer (drying method), sealing bags, and scissors. Key instrument parameters are listed in Table 1.

Table 1

Parameters of the equipment

Equipment	Parameters	Values
RGM-3005 Universal Testing Machine	Maximum Load	5 KN
	Test Speed	0.001~500 mm/min
	Accuracy	±0.5 %
Kinect v2 Camera	Resolution	1920×1080 32bits
	Frame Rate	30 fps
OHAUS Moisture Analyzer	Heating Source	Halogen lamp
	Maximum Capacity	90 g
	Accuracy	0.001 g

Test Methods

During the tensile test, the stem diameter was first measured in two perpendicular directions using a vernier caliper, and the average was taken as the stem diameter. Excluding data on significant slippage and uneven stem cracks during the stretching process, a total of 36 sets of data were recorded in the experiment. Several feature points were marked with a marker pen within a 50 mm gauge section in the middle of the 200 mm long stem. Images of these points were recorded with a camera during stretching for subsequent extraction of axial and radial strains. During the test, the stem was clamped in self-tightening wedge grips to prevent slippage. A universal testing machine was used to apply the load at a constant speed of 20 mm/min.

F_b represents the maximum breaking force endured by the stem at break. This maximum breaking force was monitored in real-time by the universal testing machine and could be read immediately after the test concluded. The moisture content of each numbered stem was measured after testing.

In this experiment, image recognition technology is employed to measure the deformation per unit length of a rapeseed stem. A camera captures images of the stem, which are marked with distinct points for precise tracking. Using MATLAB, these marked points, A and B, are digitally identified to obtain their coordinates. The axial distance between these points before the application of stress is denoted as Y_1. When the stem is stretched to its breaking force, Fb, the new distance is recorded as Y_2. Thus, the axial deformation ε_y can be calculated. Since strain is the relative deformation per unit length of the stem, the spacing between feature points does not need to be converted to actual length, only the pixel changes between feature points in the image are used to calculate. Similarly, radial deformation, ε_x can also be calculated using identified coordinates. As shown in formula (1).

$$\begin{cases} \varepsilon_y = \dfrac{Y_2 - Y_1}{Y_1} \\ \varepsilon_x = \dfrac{X_2 - X_1}{X_1} \end{cases} \tag{1}$$

Prior to the experiment, each stem is marked using a marker to assist in subsequent image recognition, as depicted in figure 2. The setup involves connecting a Kinect v2 camera to a computer, ensuring that the camera is aligned directly with the marked points on the stem.

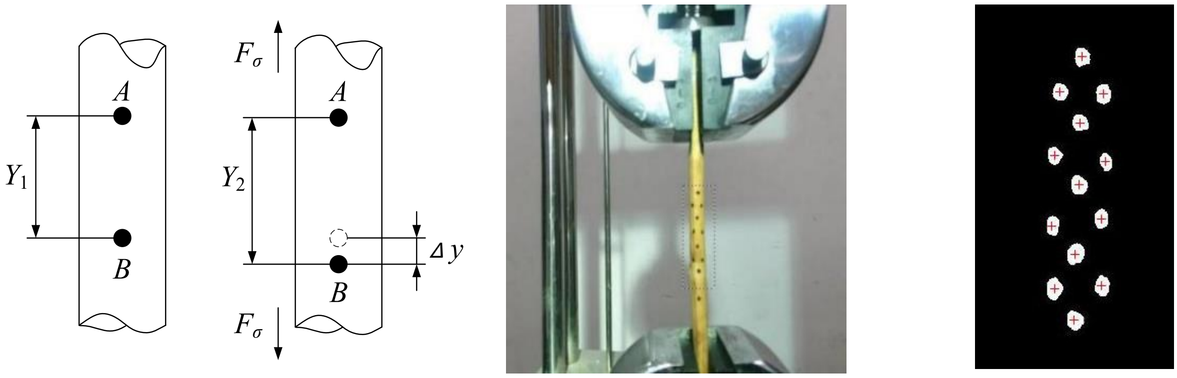

a. Axial deformation of stem b. Feature point marking c. Obtain the coordinates

Fig. 2 - Measuring orthogonal strain by digital image correlation

A caliper is employed to measure the diameter of each stem before testing. During the tensile test, the Kinect v2 camera is used continuously until the stems break, while the maximum breaking force is noted. Each broken stem is catalogued and sealed in a bag for moisture content measurement after the test. Post-experimentation, images captured by the Kinect v2 camera, both before stretching and at the point of breaking, are analyzed using image processing to calculate the radial and axial deformations of the stem. The experimental setup is illustrated in Figure 3.

Fig. 3 - Field of stem tensile test

In the tensile fracture test of rapeseed stems, significant differences were observed in the fracture modes, which can be categorized into three main types: a. Edge fracture; b. Central fracture; c. Tearing, as illustrated in figure 4.

To ensure the accuracy and comparability of experimental data, this study defines stems that exhibit a clean break through the center as the standard mode of fracture. This selection criterion is essential for excluding variations caused by edge effects or asymmetric tearing, thereby ensuring the data reflect the intrinsic tensile properties of the material.

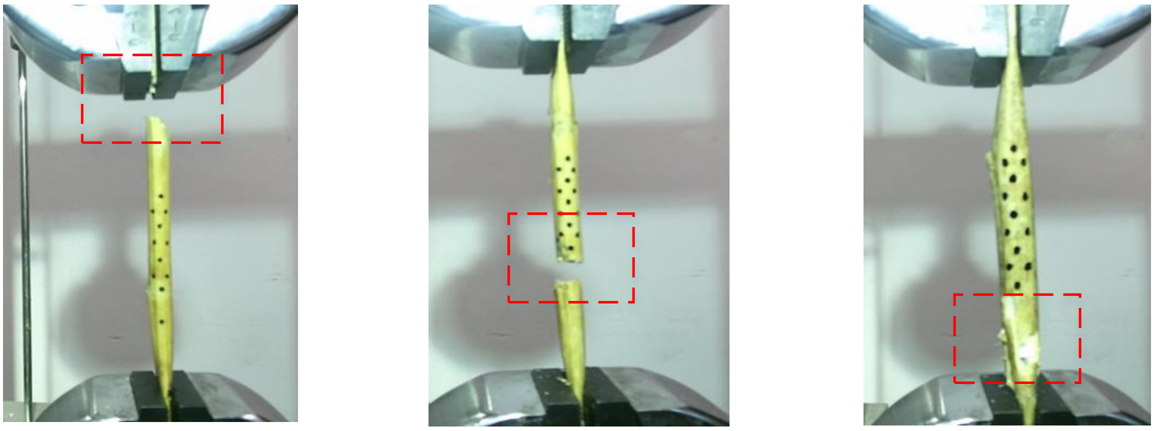

a. Edge fracture b. Central fracture c. Tearing

Fig. 4 - Images of stem before and after tensile stress

The tensile strength of rapeseed stems is primarily governed by the fiber layer, whereas the contribution of the pith layer to the tensile strength is negligible compared with that of the fiber layer. Therefore, the connected domain of the fiber layer in the cross-section of rapeseed stems was extracted through image processing to calculate the area fraction of the fiber layer. Using a standard correction version with a known side length of 1 cm as a reference, convert the pixel area to the actual area. The processing workflow is illustrated in Figure 5.

a. Rapeseed stem cross-section b. Connected domain in the cross-section c. Connected domain of the pith d. Connected domain of the fiber layer

Fig. 5 – Image processing workflow for a rapeseed stem cross-section.

The tensile strength σ_b of rapeseed stems was calculated using the following equation:

$$\sigma_b = \frac{F_b}{S} \tag{2}$$

In Equation (2), F_b is the tensile breaking force of the stem, and S is the area of the fiber layer.

$$S = S_1 - S_2 \tag{3}$$

The area of the fiber layer can be calculated using Equation (3), where S_1 is the total area of the stem cross-section and S_2 is the area of the pith layer.

RESULTS

As shown in figure 5, the tensile breaking force of stems increases with stem diameter. For rapeseed stems with diameters ranging from 7 to 16 mm, the minimum breaking force is 166.82 N and the maximum breaking force is 970.82 N. The functional relationship between stem breaking force and stem diameter d_{x1} is given in equation 4.

$$F_b = 42.064 d_{x1} - 92.894 \tag{4}$$

Figure 6 illustrates the tensile strain of rapeseed stems with different diameters. Analysis indicates that the tensile strain of the stems shows no significant correlation with stem diameter. After removing outlier data points, the average values for radial and axial strain were calculated. The average axial strain was ε_y=4.22±2.23×10^{-3}, and the average radial strain was ε_x=3.84±2.17×10^{-2}. Comparing radial strain with axial strain in stems reveals that axial deformation is significantly smaller than radial deformation. This difference is mainly attributable to the longitudinal orientation of the fiber bundles in rapeseed stems, which provides greater resistance to axial deformation. Conversely, the hollow radial structure of rapeseed stems, when subjected to axial tension, facilitates greater contraction toward the center. Therefore, to thoroughly investigate the mechanical properties of rapeseed stems, their structural characteristics must be fully accounted for. This necessitates separate studies of stem mechanical behavior along both the axial and radial directions.

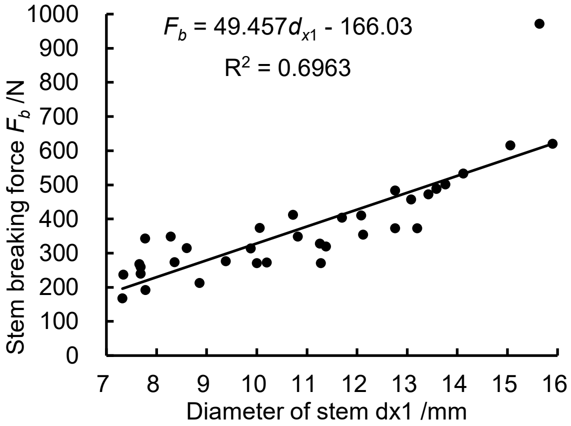

Fig. 5 - Effect of diameter on breaking force

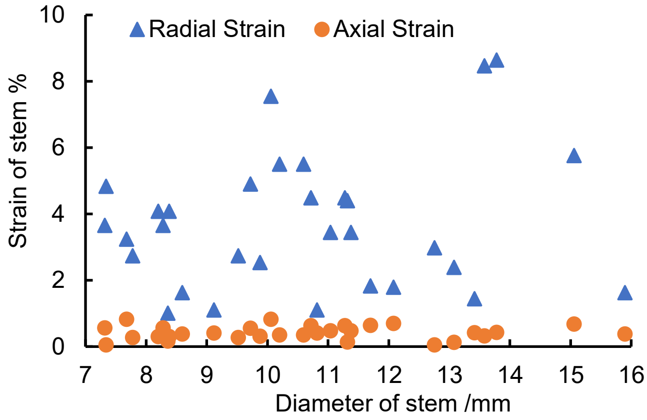

Fig. 6 - Effect of diameter on tensile strain

As shown in figure 7, the area of the rapeseed fiber layer increases with the increase of the diameter of the rapeseed stem, and an R-squared value of 0.9355 indicates a significant correlation between the area of the fiber layer and the size of the diameter. Figure 8 shows the relationship between the diameter of rapeseed stems and their tensile strength. It can be seen from the figure that the tensile strength of rapeseed stems decreases with the increase of stem diameter. The functional relationship between fiber area layer S and stem diameter d_{x1} is given in Equation 5.

$$S = 2.363 d_{x1} - 13.135 \tag{5}$$

Figure 8 shows the relationship between the diameter of rapeseed stems and their tensile strength. It can be seen from the figure that the tensile strength of rapeseed stems decreases with the increase of stem diameter. The R value of 0.6617 indicates that the trend is not very obvious, and it is difficult to maintain consistent stem moisture content during the experiment. Therefore, it is necessary to add moisture content as an influencing factor to further analyze the tensile strength of the stem.

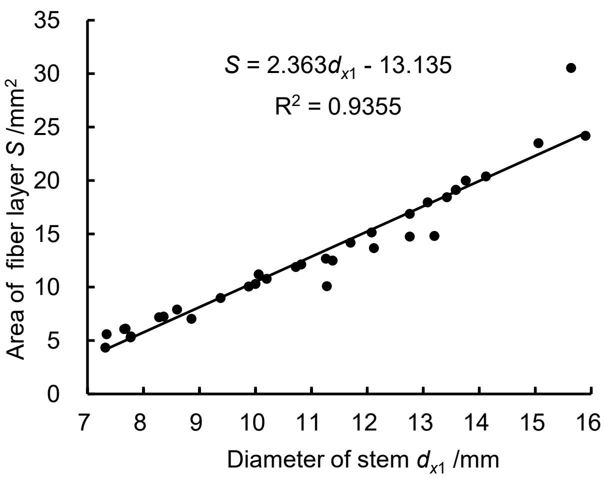

Fig. 7 - Effect of diameter on fiber area

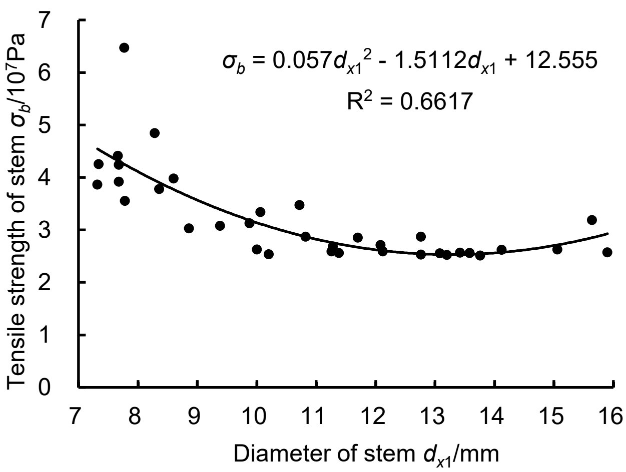

Fig. 8 - Effect of diameter on tensile strength

To investigate the combined effects of stem diameter and moisture content on tensile strength, tensile strength was measured for stems with different diameters and moisture contents, as shown in Table 2. To more clearly visualize the combined effects of stem diameter and moisture content on tensile strength, the measured data were fitted using the least-squares method to construct a three-dimensional response surface. The resulting surface plot, illustrating the relationship among stem diameter, moisture content, and tensile strength over the tested range, is presented in Figure 9.

Experimental Data from Rapeseed Stem Tensile Tests **Table 2**

Number	Mass (g)	Diameter (mm)	Tensile Breaking Force (N)	Moisture Content (%)	Tensile strength (MPa)
1	2.354	8.60	313.73	44.10	39.8
2	2.233	8.86	212.08	47.33	30.3
3	1.856	7.32	166.82	50.57	38.6
4	2.904	10.00	269.60	49.97	26.3
5	3.445	10.20	272.25	50.33	25.3
6	3.770	9.38	275.27	48.70	30.8
7	4.202	11.38	318.43	47.94	25.6
8	3.585	10.72	411.73	42.40	34.7
9	4.456	13.20	372.34	41.10	25.2
10	2.935	13.76	500.52	42.24	25.1
11	5.973	12.76	483.00	43.86	28.7
12	5.280	13.42	471.82	37.65	25.6
13	4.321	7.34	236.64	52.51	42.5
14	1.858	7.68	258.67	37.57	42.4
15	2.065	8.36	272.93	38.97	37.7
16	2.360	7.77	341.97	37.09	64.6
17	3.363	9.88	313.42	45.75	31.2
18	3.810	10.06	372.84	41.84	33.3
19	5.250	13.08	456.53	42.78	25.5
20	4.823	11.70	403.26	44.55	28.5
21	4.856	12.08	409.45	44.92	27.1
22	6.140	13.58	487.82	43.24	25.6
23	5.972	15.06	614.99	40.63	26.2
24	9.483	15.90	619.92	46.37	25.7
25	2.494	7.68	238.90	52.00	39.2
26	3.082	8.28	347.50	54.40	48.4
27	2.580	7.78	190.82	57.39	35.5
28	3.465	7.66	267.44	51.59	44.1
29	3.945	10.82	347.35	56.93	28.7
30	3.273	11.26	327.47	50.91	25.9
31	5.107	11.28	269.89	57.67	26.8
32	5.631	12.12	352.97	60.76	25.9
33	6.321	12.76	372.16	53.68	25.3
34	8.156	13.58	487.90	52.94	25.6
35	10.577	15.64	970.82	60.60	31.8
36	8.265	14.12	532.60	60.59	26.2

As shown in Figure 9, the tensile strength of rapeseed stems generally decreases with increasing stem diameter. Within the tested stem diameter range of 7–16 mm, the tensile strength exhibits considerable variability, with a minimum value of 25.1 MPa and a maximum of up to 64.6 MPa. In addition, Figure 9 comprehensively presents the combined influence of stem moisture content and diameter on tensile strength. It can be observed that changes in moisture content also alter the mechanical response of the stem material. Generally, as moisture content increases, the binding strength of hydrogen bonds between fibers and the lignin–hemicellulose matrix within the stem may weaken, leading to a decrease in tensile strength. However, the extent to which moisture content reduces tensile strength is not entirely consistent across different diameter classes; stems with larger diameters, owing to their greater structural redundancy, may be relatively less sensitive to changes in moisture content.

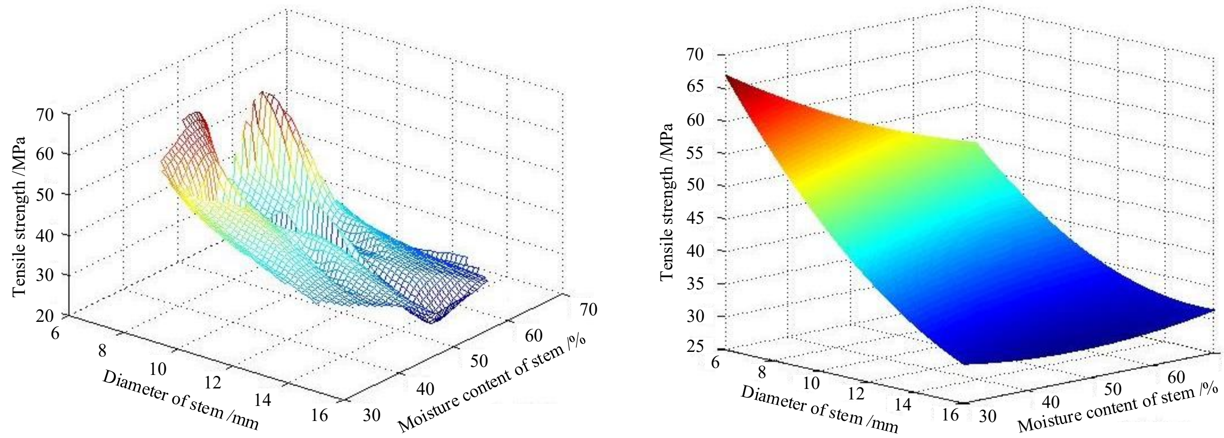

a. Mesh plot of the experimental data b. Regression equation surface plot

Fig. 9 - Effect of stem moisture content and diameter on tensile strength

Analysis indicates that both stem moisture content and diameter exert a significant influence. The experimental data were entered into EViews for optimization analysis of regression equation, where dx1 represents rapeseed stem diameter, dx_2 represents stem moisture content, and C denotes the constant term. The correlation test results of variables are shown in Table 3, the results show that the correlation coefficients between $\mathbf{d_{x1}\ d_{x2}}$ and $\mathbf{d_{x1}}$, as well as between $\mathbf{d_{x1}^2\ d_{x2}^2}$ and $\mathbf{d_{x1}}$, are all greater than 0.8, indicating strong collinearity. Therefore, the interaction term is not included in the regression model. The results of the analysis of variance for the experimental data are presented in Table 4.

Table 3

Correlation test results of variables

Variable	d_{x1}	d_{x2}	d_{x1}^2	d_{x2}^2	$d_{x1}\ d_{x2}$	$d_{x1}^2\ d_{x2}^2$
d_{x1}	1.0000	0.0278	0.9944	0.0404	0.8419	0.7963
d_{x2}	0.0278	1.0000	0.0323	0.9975	0.5478	0.5591
d_{x1}^2	0.9944	0.0323	1.0000	0.0463	0.8408	0.8063
d_{x2}^2	0.0404	0.9975	0.0463	1.0000	0.5614	0.5793
$d_{x1}\ d_{x2}$	0.8419	0.5478	0.8408	0.5614	1.0000	0.9849
$d_{x1}^2\ d_{x2}^2$	0.7963	0.5591	0.8063	0.5793	0.9849	1.0000

Table 4

Regression analysis of experimental data

Variable	Coefficient	Std. Error	t-Statistic	Prob.
C	23.9645	4.1115	5.8287	0.0000
d_{x1}	-1.3803	0.2942	-4.6921	0.0001
d_{x1}^2	0.0505	0.01315	3.8367	0.0006
d_{x2}	-0.4815	0.1679	-2.8684	0.0074
d_{x2}^2	0.0047	0.0018	2.7564	0.0097
R2	0.7483	**Mean dependent var**		3.1924
Adjusted R2	0.7158	**S.D. dependent var**		0.8628
S.E of regression	0.4600	**Akaike info criterion**		1.4130
Sum squared resid	6.5593	**Schwarz criterion**		1.6329
F-statistic	23.0361	**Hannan-Quinn criterion**		1.4898
Prob(F-statistic)	0.0000	**Durbin-Watson stat**		2.3786

The experimental data were processed using stem diameter d_{x1} and stem moisture content d_{x2} as variables to perform a quadratic polynomial regression analysis on tensile strength σ_b, yielding the regression equation 6.

$$\sigma_b = -1.3803 d_{x1} - 0.4815 d_{x2} + 0.0505 d_{x1}^2 + 0.0047 d_{x2}^2 + 23.9645 \quad (6)$$

CONCLUSIONS

Axial tensile tests combined with digital image correlation (DIC) systematically revealed the fundamental relationships among stem diameter, moisture content, and the fracture behavior of tensile strength. The breaking force exhibited a strong linear increase with stem diameter, whereas the tensile strength was well described by a quadratic response surface model as a function of both stem diameter and moisture content. Most notably, DIC strain measurements demonstrated pronounced mechanical anisotropy: the radial strain was approximately an order of magnitude larger than the axial strain, strongly indicating a lateral-dominated deformation mechanism prior to failure. Nevertheless, it should be emphasized that these quantitative results are subject to inevitable measurement uncertainties. Primary sources of error include the inherent biological variability among specimens, micro-slippage at the clamping interfaces, local moisture gradients within the stem tissue, and intrinsic noise in the DIC strain computation. Consequently, although the reported trends are considered physically meaningful, the absolute force and strain values should be applied with due caution when high precision is required.

Despite the above limitations, the strongly anisotropic strain behavior suggests that threshing elements designed to induce multi-axial stress states—such as combined bending, shear, and compression—rather than simple uniaxial tension, could more effectively suppress uncontrolled stem fracture, potentially contributing to reduced grain loss and improved seed cleanliness, pending further validation under dynamic and field conditions. These findings thus establish a critical bridge between the biomechanical properties of oilseed rape stems and the engineering optimization of combine harvester threshing units. Future work should progress beyond the quasi-static conditions employed here to dynamic loading regimes that better replicate the complex impact and bending actions encountered inside a threshing chamber. A systematic investigation of additional influential factors—including varietal differences, the maturity gradient along the stem, and internode position—is essential to enhance the generality and predictive power of the developed models. Furthermore, integrating the experimentally measured mechanical parameters into finite element simulations of the stem–threshing element interaction will enable virtual prototyping and parametric optimization. Coupling such simulations with field validation and real-time sensing of stem diameter and moisture content could lay the foundation for adaptive control strategies that autonomously regulate threshing parameters. Ultimately, this integrated approach holds great promise for achieving more efficient and cleaner rapeseed combine harvesting.

ACKNOWLEDGEMENT

The authors gratefully acknowledge the support of the affiliated institution and the technical assistance provided during the research. Appreciation is also extended to the research group members for their valuable discussions. This project was funded by the Hubei Natural Science Foundation of China (2025AFB006).

REFERENCES

[1] Cujbescu, D., Găgeanu, I., & Iosif, A. (2021). Mathematical modeling of ear grain separation process depending on the length of the axial low threshing apparatus. *INMATEH–Agricultural Engineering*. 65, 101–110.

[2] Fang, Z., Yu, J., Yang, F., Sheng, Y., Rao, J., & Zheng, Z. (2026). Tensile and fatigue tests of steel specimens based on digital image correlation. *Progress in Steel Building Structures*, 1-10.

[3] Guan, Z., Mu, S., Li, H., Jiang, T., Zhang, M., & Wu, C. (2022). Flexible DEM model development and parameter calibration for rape stem. *Applied Sciences*, 12(17), 8394.

[4] Guo, H., Guo, L., Li, H., Dong, Y., Zhou, W., & Han, J. (2024). Calibration and experiment of the discrete element simulation parameters for rapeseed stems during the suitable harvest period. *Transactions of the Chinese Society of Agricultural Engineering*, 40(24), 20-29.

[5] Han, M., Li, M., Duan, H., Xu, K., & Yu, K. (2024). Rigid-flexible coupling simulation and experiment of plant stem clamping device based on ADAMS. *Transactions of the Chinese Society for Agricultural Machinery*, 55(2), 109-118.

[6] Hu, Y., Javed, H., Liu, L., Alabdallah, N., Ghaffor, K., & Liu, Y., Luo, Y., Gulzar, F., Peng, X., & Wu, Y. (2025). Evaluate the sensitivity of rapeseed lodging under low light: a field study on the biomechanics of stem and root lodging in rapeseed (*Brassica napus l.*). *Field Crops Research*, 327.

[7] Li, Z., Luo, H., Wang, X., Li, Y., Zhang, S., & Tong, X. (2025). Design and optimization of transverse differential speed conveying device for horizontal rapeseed windrower. *Journal of Jiangxi Agricultural University*, 47(2), 486-504.

[8] Lian, G., Wei, X., Ma, L., Zhou, G., & Zong, W. (2022). Design and experiments of the axial-flow spiral-drum threshing device for the edible sunflower. *Transactions of the Chinese Society of Agricultural Engineering*, 38(17), 42–51.

[9] Mazzilli, SR., & Verocai, M. (2024). A comparative study of yield components and their trade-off in oilseed crops (*Brassica napus l*. and brassica carinata a. braun). *European Journal of Agronomy*.

[10] Parvin, A., Rahman, M., & Cattani, DJ. (2021). The effect of stem diameter on the *Brassica napus* (type: canola) (cultivar: HYHEAR 3) fiber quality. *World Journal of Engineering and Technology*, 09(3):458-481.

[11] Qing, Y., Li, Y., Xu, L., & Ma, Z. (2021). Study on the rape pod shatter resistance suitable for low-loss harvesting of harvester reel. *INMATEH–Agricultural Engineering*, 63(1).

[12] Ren, S., Wu, M., Xie, F., & Guan, C. (2014). Study on viscoelastic properties of rapeseed stem and the constitutive relationship. *Journal of Anhui Agricultural Sciences*, 42(35), 12749-12751.

[13] Shan, Y., Liao, Q., Yuan, J., Wan, X., & Liao, Y. (2024). Effects of cutting parameters on the shearing properties of oilseed rape (*Brassica Napus L*.) shoots in harvesting. *Applied Engineering in Agriculture*, 40(3):339-349.

[14] Shu, C., Yi, P., Wu, C., Wan, X., Liao, Q., & Yuan, J. (2025). Design and experiment of lightweight and simple threshing machine in hilly areas for rapeseed. *Transactions of the Chinese Society of Agricultural Engineering*, 41(19), 54-64.

[15] Sikorska, A., Gugaa, M., Zarzecka, K., Mystkowska, I., Ginter, A., Findura, P., & Pristavka, M. (2023). Biometric characteristics of winter rape plants (*Brassica napus l*.) before harvest in the soil and climatic conditions of north-eastern Poland. PLoS ONE (v.1;2006), 023, 18(8):14.

[16] Sun, X., Zong, W., Ma, L., & Wan, X. (2025). Design and test of the dual-airduct cleaning device for oilseed rape harvesters in hilly and mountainous areas. *Transactions of the Chinese Society of Agricultural Engineering,* 41(13), 72-82.

[17] Sun, Y., Jiao, Z., Huang, J., Dai, L., Sun, R., Hu, X., Liang, Z., Xue, Y., & Xu, Z. (2026). Current status and research progress in the utilization of oilseed rape straw as feed in China. *Chinese Journal of Oil Crop Sciences*, 1-7.

[18] Tang, Q., Jiang, L., Yu, W., Wu, J., & Wang, G. (2024). Design and experiment of high moisture corn threshing device with low damage. *INMATEH–Agricultural Engineering*, 74(3), 172-183.

[19] Vlăduț, N., Biriş, S., Cârdei, P., Găgeanu, I., Cujbescu, D., Ungureanu, N., Popa, L., Perişoară, L., Matei, G., & Teliban, G. (2022). Contributions to the mathematical modeling of the threshing and separation process in an axial flow combine. *Agriculture*, *12*, 1520.

[20] Vlădut, N., Ungureanu, N., Biris, S., Voicea, I., Nenciu, F., Găgeanu, I., Cujbescu, D., Popa, L., Boruz, S., Matei, G., Ekielski, A., & Teliban, G. (2023). Research on the identification of some optimal threshing and separation regimes in the axial flow apparatus. *Agriculture*, 13(4), 838.

[21] Wang, C., Wang, S., Xie, L., Liu, Y., Deng, J., & He, W. (2023). Fatigue crack growth behavior of marine steel under variable amplitude loading-combining DIC technique and SEM observation. *International Journal of Fatigue*, 170, 107508.

[22] Xiao, R., Su, H., Liao, Y., Wang, H., Sheng, Y., Rao, J., & Zheng, Z. (2026). Study on MOE and MOR of bamboo-wood composite panels with different core materials. *Journal of Central South University of Forestry & Technology*, 1-9.

[23] Yuan, J., Liao, Q., Wan, X., Yang, J., & Shu, C. (2024). Parameter matching and experiment of the combined cyclone separation and cylinder sieve cleaning system for rape combine harvester. *International Journal of Agricultural & Biological Engineering*, 17(1), 128–136.

[24] Zhan, G., Liu, W., & Zhang, P. (2025). Study on the movement characteristics of rapeseed threshing materials based on dem simulation and high-speed imaging. *INMATEH–Agricultural Engineering*, 76(2), 1279-1288.

[25] Zhang, M., Xu, C., Li, C., Wang, G., Yang, Y., & Jiang, T. (2025). Parameter optimization and experiment of a single longitudinal axial flow full-circumference separation threshing device for rapeseed harvester. *INMATEH – Agricultural Engineering*, 76(2), 1231-1243.

[26] Zhou, J., Liao, Q., Wan, X., Yuan, J., Li, J., & Qin, Y. (2025). Discrete element simulation of grain crushing and optimization of chopping and throwing device for rapeseed combine harvester. *Journal of Huazhong Agricultural University*, 44(1), 265-275.